



## Greenland meltwater storage in firn limited by near-surface ice formation

**Machguth, Horst; MacFerrin, Mike; van As, Dirk; Box, Jason E.; Charalampidis, Charalampos; Colgan, William; Fausto, Robert S.; Meijer, Harro A. J.; Mosley-Thompson, Ellen; van de Wal, Roderik S. W.**

*Published in:*  
Nature Climate Change

*Link to article, DOI:*  
[10.1038/NCLIMATE2899](https://doi.org/10.1038/NCLIMATE2899)

*Publication date:*  
2016

*Document Version*  
Peer reviewed version

[Link back to DTU Orbit](#)

### *Citation (APA):*

Machguth, H., MacFerrin, M., van As, D., Box, J. E., Charalampidis, C., Colgan, W., Fausto, R. S., Meijer, H. A. J., Mosley-Thompson, E., & van de Wal, R. S. W. (2016). Greenland meltwater storage in firn limited by near-surface ice formation. *Nature Climate Change*, 6(4), 390-395. <https://doi.org/10.1038/NCLIMATE2899>

---

### General rights

Copyright and moral rights for the publications made accessible in the public portal are retained by the authors and/or other copyright owners and it is a condition of accessing publications that users recognise and abide by the legal requirements associated with these rights.

- Users may download and print one copy of any publication from the public portal for the purpose of private study or research.
- You may not further distribute the material or use it for any profit-making activity or commercial gain
- You may freely distribute the URL identifying the publication in the public portal

If you believe that this document breaches copyright please contact us providing details, and we will remove access to the work immediately and investigate your claim.

# Greenland meltwater storage in firn limited by near-surface ice formation

Horst Machguth<sup>1,2,\*</sup>, Mike MacFerrin<sup>3</sup>, Dirk van As<sup>1</sup>, Jason E. Box<sup>1</sup>, Charalampos Charalampidis<sup>1,4</sup>, William Colgan<sup>1,5</sup>, Robert S. Fausto<sup>1</sup>, Harro A.J. Meijer<sup>6</sup>, Ellen Mosley-Thompson<sup>7</sup> and Roderik S. W. van de Wal<sup>8</sup>

<sup>1</sup> Geological Survey of Denmark and Greenland GEUS, DK-1350 København K, Denmark

<sup>2</sup> Centre for Arctic Technology, Technical University of Denmark, DK-2800, Kgs. Lyngby, Denmark

<sup>3</sup> Cooperative Institute for Research in Environmental Sciences (CIRES), University of Colorado at Boulder, Boulder, USA

<sup>4</sup> Department of Earth Sciences, Uppsala University, 752 36 Uppsala, Sweden

<sup>5</sup> Department of Earth and Space Science and Engineering, York University, Toronto, Ontario, M3J 1P3, Canada

<sup>6</sup> Centre for Isotope Research (CIO), Energy and Sustainability Research Institute Groningen (ESRIG), University of Groningen, NL-9747AG Groningen, the Netherlands

<sup>7</sup> Byrd Polar and Climate Research Center and Department of Geography, The Ohio State University, Columbus OH, 43210, USA

<sup>8</sup> Institute for Marine and Atmospheric Research Utrecht (IMAU), University of Utrecht, NL-3584CC Utrecht, the Netherlands

\*Now at: Department of Geography, University of Zurich, Zurich, Switzerland

Approximately half of Greenland's current annual mass loss is attributed to runoff from surface melt<sup>1</sup>. At higher elevations, however, melt does not necessarily equal runoff, because meltwater can refreeze in the porous near-surface snow and firn<sup>2</sup>. Two recent studies suggest that all<sup>3</sup> or most<sup>3,4</sup> of Greenland's firn pore space is available for meltwater storage, making the firn an important buffer against contribution to sea level rise for decades to come<sup>3</sup>. Here, we employ *in-situ* observations and historical legacy data to demonstrate that surface runoff begins to dominate over melt water storage well before firn pore space has been completely filled. Our observations frame the recent exceptional melt summers in 2010 and 2012<sup>5,6</sup>, revealing significant changes in firn structure at different elevations caused by successive intensive melt events. In the upper regions (above ~1900 m a.s.l.), firn has undergone substantial densification, while at lower elevations, where melt is most abundant, porous firn has lost most of its capability to retain meltwater. Here, the formation of near surface ice layers renders deep pore space difficult to access, forcing meltwater to enter an efficient<sup>7</sup> surface discharge system and intensifying ice sheet mass loss earlier than previously suggested<sup>3</sup>.

In Greenland's accumulation area, porous firn up to 80 meters thick underlies the ice sheet surface<sup>8</sup>. While the majority of the contemporary firn extent experienced limited melt in the past, recent exceptional melt events now reach the highest parts of the ice sheet<sup>5</sup>. Consequently, the percolation area, where the infiltration of surface meltwater into the firn redistributes mass vertically and horizontally<sup>9</sup>, is expanding. It is estimated that currently 30-40% of melt is retained in the firn<sup>1,4</sup>.

However, direct quantifications are subject to large uncertainties, and understanding feedback mechanisms in Greenland's changing firn is vital to assess and project ice sheet mass balance.

Meltwater percolating in firn can be retained as liquid by capillary forces<sup>10</sup>, in firn aquifers<sup>11</sup>, or by refreezing in firn pore space, whereby refrozen meltwater forms ice horizons or lenses<sup>12</sup>. If cold content and unfilled pore space are available, refreezing is very efficient for long term meltwater retention<sup>13</sup> and thus buffers mass loss<sup>2,13</sup>. A recent study<sup>3</sup> postulates two end-member pathways of the uncertainty in calculating this buffer, with meltwater either percolating deep into the firn, eventually consuming all pore space, or aggregating in low permeability ice layers near the surface that render underlying pore space unavailable to further refreezing. Field data from the years 2007 to 2009<sup>14</sup>, suggested the prior is more likely, implying that firn will remain an important meltwater buffer in coming decades<sup>3,4</sup> and that substantial runoff from the percolation area starts once all firn pore space is filled<sup>3</sup>.

In summer 2012, Greenland experienced the largest observed melt extent on record<sup>5</sup>. Satellite images (Fig. 1 and Supplementary Figs. 1 and 2) of the western flank of the ice sheet at 67°N show meltwater runoff channels reached to unprecedented elevations ~300 m above and ~25 km east of the longer term equilibrium line altitude (1550 m a.s.l.<sup>15</sup>), implying the limits of firn retention had been reached. Here, we employ in-situ data to characterize the state of the firn in this region and quantify the impact of large melt on the partitioning between advection (i.e. surface runoff) and diffusion (i.e. percolation) of water. Our data include 26 firn cores drilled primarily along a transect at 67°N in West Greenland (see Methods and Fig. 1). Cores were drilled in spring 2009, 2012, 2013 and 2015, and thus bracket two recent extraordinary melt seasons of 2010 and 2012. Firn temperatures were monitored at one site and a 110 km firn radar transect connects the cores. These recent cores are compared with cores drilled in 1997 and 1998 to assess changes in firn properties over the past ~15 years.

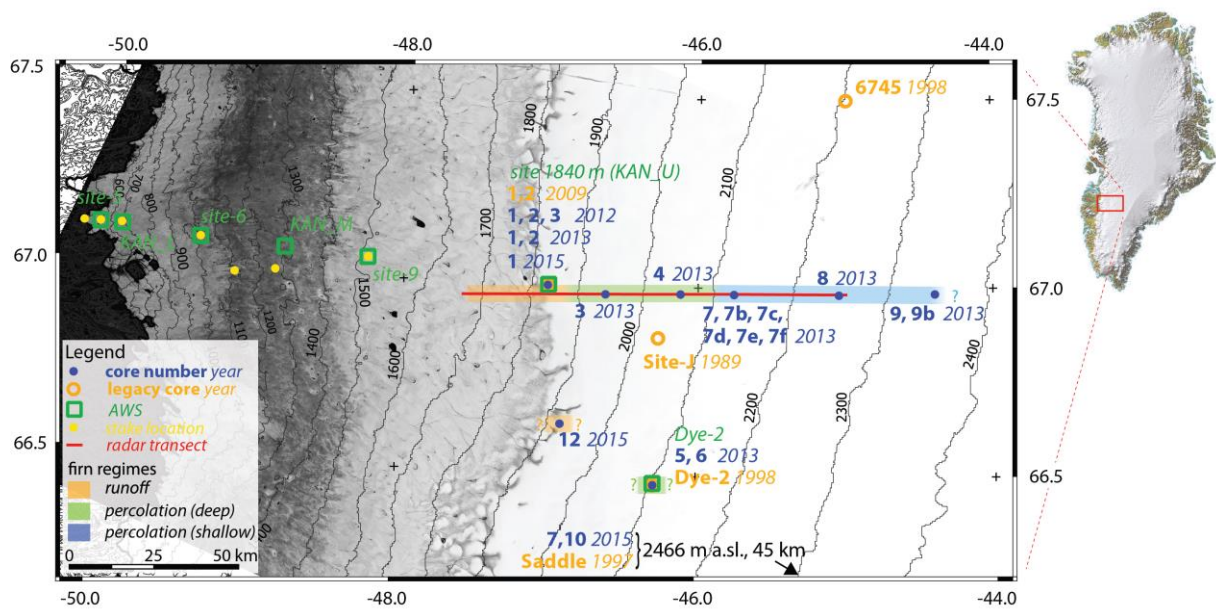


**Figure 1** | Map illustrating the firn core sites and main radar transect. Cores collected within our project are in blue, legacy cores are in orange, automatic weather stations are denoted in green. In the background is a panchromatic Landsat 7 image from July 16 2012. Landsat image: USGS/Nasa.

The 2013 cores (Fig. 2) reveal two statistically distinguishable patterns in firn stratigraphy (see Methods), hereafter referred to as ‘firn regimes’: (1) At elevations >1900 m a.s.l. the firn column contains ice lenses whose average thickness and amount decreases with elevation. Active percolation of meltwater takes place in this zone<sup>14</sup> which we accordingly term the “firn percolation regime.” (2) At 1840 m a.s.l. a ~5.5 m thick near surface ice layer overlies porous firn. The layer is not a local phenomenon and is clearly recognizable in radar profiles (see Methods) where it is continuously traced both locally on a 1 x 1 km radar grid, and regionally from the lowermost appearance of porous firn (~1680 m a.s.l.) to ~1870 m a.s.l. (Supplementary Fig. 3). A similar firn stratigraphy is also found in a core drilled 50 km further south, close to the local summer 2012 runoff limit (Fig. 1 and Supplementary Fig. 4). Below, we show that meltwater in the zone of thick near-surface ice layers is dominated by advection, rather than by diffusion, and we thus apply the term “firn runoff regime”.

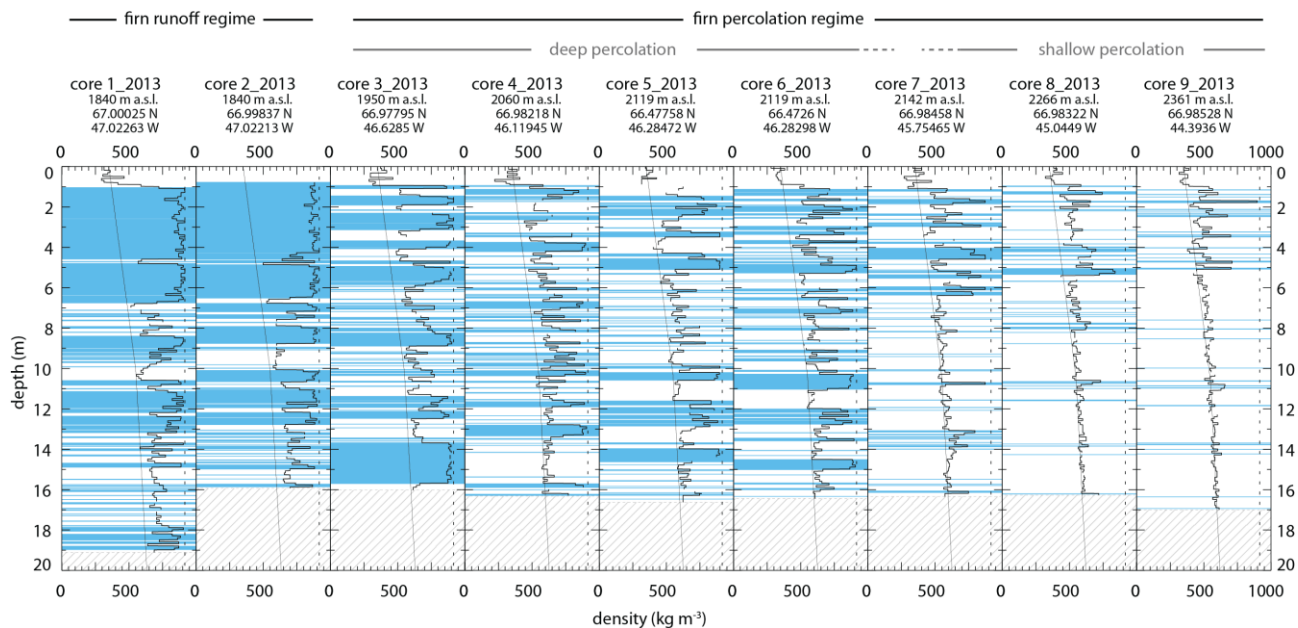


**Figure 2** | Stratigraphy of the nine major firn cores drilled in late April to mid May 2013. Ice lenses are in blue and given at 1 cm vertical resolution. Density at 10 cm resolution is in black. The dotted vertical line indicates the density of pure ice ( $917 \text{ kg m}^{-3}$ ); the thin inclined line denotes dry firn density according to [8]. Dashed areas mark the end of the cores. The association of each core with the hypothesized firn regimes is indicated at the top.

Comparing 2013 and 2015 firn density profiles to analogous 2012, 2009, 1998 and 1997 profiles reveals characteristics in melt water percolation and their changes over time (Fig. 3). While the 2012 and 2009 data represent the state immediately prior to the extraordinary melt summers of 2012 and 2010, respectively, the 1997/1998 cores<sup>16</sup> were drilled early in the recent period of strong warming in west Greenland that started in the mid-1990s<sup>1,17</sup>. Comparing 1997/1998 and 2013/2015 cores located in the upper part of the percolation regime (2466 m a.s.l.) we find a mean density increase of  $46 \text{ kg m}^{-3}$  in the top 7 m of firn (1 to 8 m depth) and  $15 \text{ kg m}^{-3}$  between 8 and 16 m depth; at 2250 m a.s.l. density increased by  $\sim 100 \text{ kg m}^{-3}$  (1 to 8 m depth) and  $18 \text{ kg m}^{-3}$  below (8 m to 12.6 m core bottom-depth). Surface meltwater generated in the recent summers refroze as ice lenses in the upper half of the cores. The ice lenses are thin and sparse, indicating limited melt, all of which the firn is capable of retaining locally. Comparing 1998 and 2013 cores in the lower part of the percolation firn regime (2120 m a.s.l.) indicate an increase in mean density of  $\sim 142 \text{ kg m}^{-3}$  in the top 7 m of firn and  $\sim 102 \text{ kg m}^{-3}$  increase at 8 to 16 m depth. Density around the 1998 surface layer (now at  $9.5 \pm 1$  m depth) has increased more than would result from dry firn compaction alone

(cf. Fig. 2), indicating that post-1998 ice lenses are now present in pre-1998 firn. We interpret this as evidence of deep (>10 m) meltwater percolation<sup>14</sup> that has modified firn stratigraphy over the entire depth of the 2013 cores (Fig. 3). Limited amounts of subsurface runoff cannot be ruled out where deep percolation prevails<sup>11,14,18</sup>.

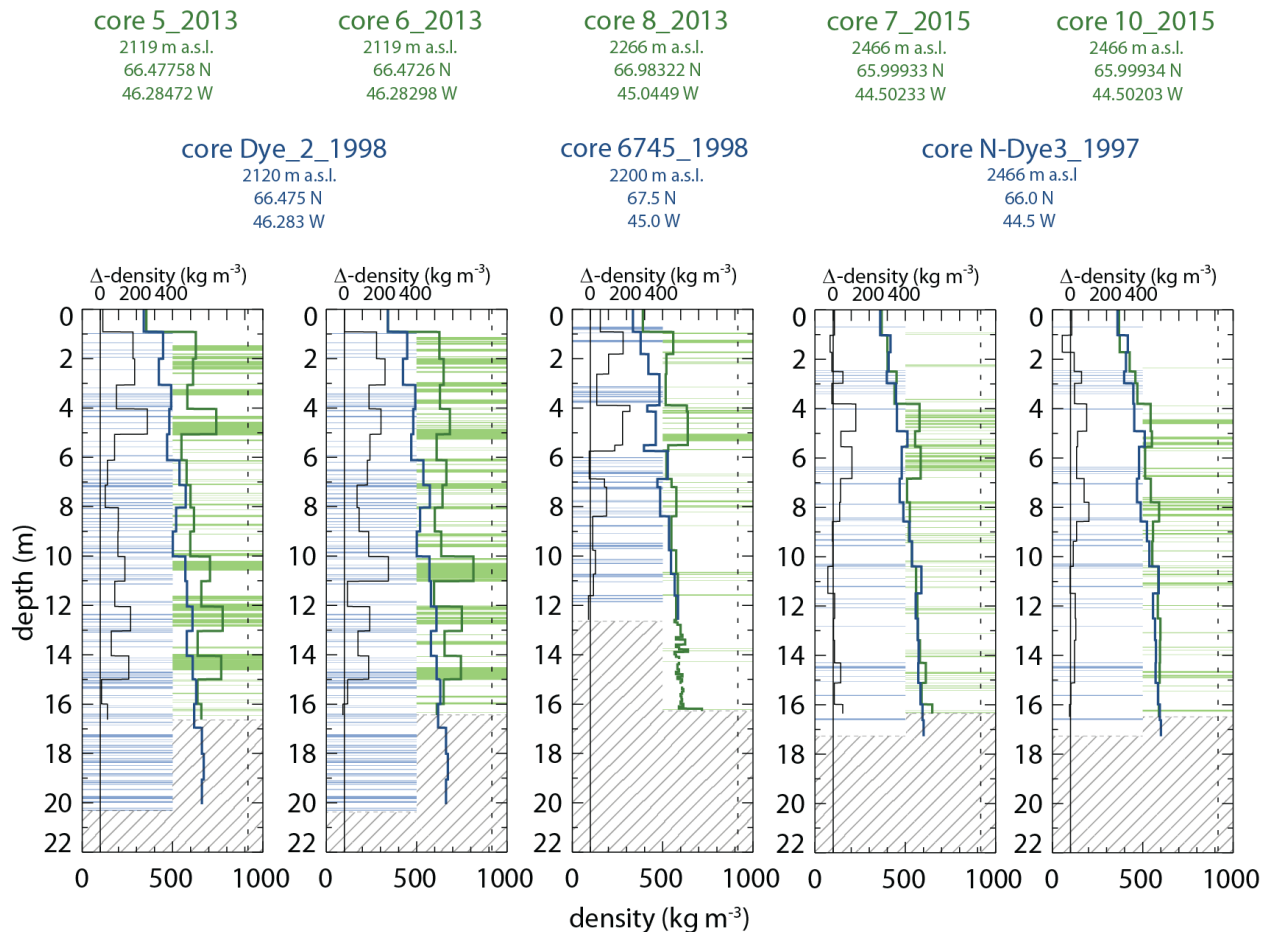


**Figure 3** | Changes in firn density (black) from 1997 or 1998 [16] (blue) to 2013 or 2015 (green). Ice lenses are shown as pale blue (1997, 1998) and pale green (2013, 2015) horizontal lines. Note that core\_8\_2013 and core\_6745\_1998 are separated by ~50 km horizontally and a ~60 m elevation difference. 1998 and 1997 coordinates are of limited accuracy. Legacy core elevations were derived using available coordinates<sup>16</sup> and a recent DEM<sup>26</sup>. Potential vertical displacements of drill sites since 1998 are insignificant due to low surface velocities (at Dye-2 ~30 m/a) and very low surface slopes.

Pronounced temporal changes in the firn towards a runoff regime are illustrated using cores from 2009 and 2012 at 1840 m.a.s.l (Supplementary Fig. 4). The date of initiation of the thick ice layers observed in 2012 cannot be established, but the two 2009 shallow cores indicate that the uppermost ~2.5 m of the firn contained a small amount of ice (~14%) in 2009. After 2009, and before spring 2012, near-surface meltwater storage exceeded the creation of new pore space, shown by the ice content in the uppermost 2.5 m of firn increasing to 60%. Pore space located below the depth of the shallow 2009 cores was likely filled as well, but in 2012 the firn below the bottom of the ice layers (~7 m depth, cf. Fig. 2) is still of similar appearance to the firn percolation regime. This indicates that deep percolation prevailed prior to the build-up of the near-surface ice layers, and that during the transition from percolation to runoff regime the traces of the former were preserved at depth.

Comparing stratigraphy and density profiles from May 2012 to 2013 in the firn runoff regime (Supplementary Fig. 4) shows that  $0.92 \pm 0.1$  m water equivalent (w.e.) of surface meltwater was generated in summer 2012, but only  $0.23 \pm 0.1$  m w.e. refroze within the subsurface, forcing  $0.69 \pm 0.15$  m w.e. (or  $75 \pm 15\%$ ) of the total melt to exit the location as runoff (see Methods). Hereafter the term *runoff* refers to water that is not retained locally and enters an efficient<sup>7</sup> surface discharge system (Supplementary Fig. 1). The core comparison also indicates that in summer 2012, refreezing filled firn layers down to ~5 m depth (Supplementary Fig. 4). Temperatures measured to 15 m depth confirm percolation to 5 m depth in September (Supplementary Fig. 5). Neither the core comparison nor the firn temperature data show signs of significant 2012 percolation below the base of the thick ice layer. Firn underlying the ~5.5 m thick ice layer is effectively isolated from subsequent percolation, even from extraordinary events such as in 2012. Now difficult to access, this “relict” pore space below the thick ice layer comprises, at the 1840 m site,  $32 \pm 10\%$  of the total pore space that would exist in a hypothetical situation with dry firn compaction alone (see Methods).

The low permeability of the thick near-surface ice layers is corroborated by a network of summer 2012 surface meltwater channels (Fig. 1 and Supplementary Fig. 1), extending over the entire zone of the firn runoff regime up to an unprecedented elevation of ~1850 m a.s.l. (see Methods and Supplementary Fig. 2). Satellite imagery and the radar transect document that 100 m-wide braided supraglacial rivers flow atop the ice layers (Supplementary Figs. 1 and 3), providing further evidence that underlying relict pore space is effectively isolated in 2012. Using elevation profiles of

surface melt and hypsometry, we quantify, on a regional scale, how the transition from percolation to firn runoff regime increases ice sheet discharge (see Methods). The calculation indicates that  $11\pm 4\%$  of total regional runoff of the 2012 melt season originated from the elevation range of the firn runoff regime. We thus conclude that changing firn regimes played a significant role in extraordinary proglacial discharge observed in the region<sup>7</sup>.

Based on in-situ data we have documented a pathway of firn response to recent warming. At higher elevations, firn density and ice lens frequency have increased due to active melt water retention, including processes of deep percolation<sup>3,14</sup>. At lower elevations, where melt is most abundant, thick near-surface ice layers have formed which limit deep percolation, render existing deep pore space difficult to access and force the majority of meltwater to migrate along the surface. In contrast to suggestions arising from previous research<sup>3</sup>, we find complete pore space filling is not a prerequisite to intensive surface runoff. Instead, the latter occurs as soon as firn conditions correspond approximately to the lower end member scenario of firn buffering capacity outlined in [3] (i.e. only the uppermost 10 m of firn pore space are available to retain melt), with the implication of shortening the estimated timing of sea level rise contribution from the percolation area.

Our conclusions refer to the impact of near surface ice layers under the extraordinary melt conditions of summer 2012; partitioning of surface migration and percolation could be different during gentle melt seasons. Comparing 2013 and 2015 stratigraphy at the 1840 m site (Supplementary Fig. 4 and Methods) indicates that melt generated during the moderate melt seasons of 2013 and 2014 has partly accreted as superimposed ice on top of the ice layer. Melt rivers originate at high elevations in both summers (Supplementary Fig. 2), providing further evidence that even limited quantities of water now mainly migrated along the surface.

Our findings relate to one transect and do not allow interference on the impact of changing firn regimes at the ice sheet scale. However, similar changes in firn structure are observed in the Canadian Arctic<sup>19,20,21</sup>. A study of Greenland's percolation area 250 km north of our study site also indicates ice formation in the near surface<sup>22</sup>. Common to these sites and our study region is the onset of substantial melt under relatively cold and dry climatological conditions. As these are



typical for the majority of Greenland's percolation area, it appears unlikely that documented changes, and their related impact, are solely of local origin.

Provided persistent climate warming<sup>23</sup>, the firn runoff regime will likely migrate to higher elevations<sup>24</sup>. Due to amplifying feedback processes, surface runoff from the zone of thick near-surface ice layers is anticipated to increase beyond its 2012 contribution (11±4% of total regional runoff). First, the ice sheet becomes flatter as elevation increases, exposing greater areas to runoff given a step change in the upper boundary of the firn runoff regime. Second, the related emergence of slush fields and runoff channels decreases surface albedo, creating additional melt in these newly saturated regions<sup>25</sup>. The combination of these factors provides firn transition with powerful leverage on Greenland's future mass balance and contribution to sea level rise.

#### References (Main text and figure captions)

- [1] van den Broeke, M. *et al.* Partitioning Recent Greenland Mass Loss. *Science* **326**, 984-986 (2009).
- [2] Pfeffer, W., Meier M. and Illangasekare, T.H. Retention of Greenland Runoff by Refreezing: Implications for Projected Future Sea Level Change. *J. Geophys. Res.* **96**, 22117-22124 (1991).
- [3] Harper, J., Humphrey, N., Pfeffer, W.T., Brown, J. and Fettweis, X. Greenland ice-sheet contribution to sea-level rise buffered by meltwater storage in firn. *Nature* **491**, 240-243 (2012).
- [4] van Angelen, J.H., Lenaerts, J.T.M., van den Broeke, M.R., Fettweis, X. and van Meijgaard, E. Rapid loss of firn pore space accelerates 21st century Greenland mass loss. *Geophys. Res. Lett.* **40**, 2109-2113 (2013).
- [5] Nghiem, S.V., *et al.* The extreme melt across the Greenland ice sheet in 2012. *Geophys. Res. Lett.* **39**, L20502 (2012).
- [6] van As, D., *et al.* Large surface meltwater discharge from the Kangerlussuaq sector of the Greenland ice sheet during the record-warm year 2010 explained by detailed energy balance observations. *Cryosphere* **6**, 199-209 (2012).
- [7] Smith, L.C., *et al.* Efficient meltwater drainage through supraglacial streams and rivers on the southwest Greenland ice sheet. *Proc. Natl. Acad. Sci. U.S.A.* **112** (2015).

- [8] Herron, M. and Langway, J.C. Firn densification: an empirical model. *J. Glaciol.* **25**, 373-385 (1980).
- [9] Brown, J., Harper, J., Pfeffer, W., Humphrey N.F. and Bradford, J. High Resolution Study of Layering within the Percolation and Soaked Facies of the Greenland Ice sheet. *Ann. Glaciol.* **52**, 35-41 (2011).
- [10] Colbeck, S.C. A study of glacier flow for an open-pit mine: an exercise in applied glaciology. *J. Glaciol.* **13**, 401-414 (1974).
- [11] Forster, R.R., *et al.* Extensive liquid meltwater storage in firn within the Greenland ice sheet. *Nature Geosci.* **7**, 95-98 (2013).
- [12] Benson, C.S. *Stratigraphic Studies in the Snow and Firn of the Greenland Ice Sheet.* CRREL Research Report 70 (1962).
- [13] Pfeffer, W. and Humphrey, N. F. Formation of ice layers by infiltration and refreezing of meltwater. *Ann. Glaciol.* **26**, 83-91 (1998).
- [14] Humphrey, N.F., Harper, J.T. and Pfeffer, W.T. Thermal tracking of meltwater retention in Greenland's accumulation area. *J. Geophys. Res.* **117**, F01010 (2012).
- [15] Van de Wal, R.S.W., *et al.* Twenty-one years of mass balance observations along the K-transect, West Greenland. *Earth Sys. Sci. Data* **4**, 31-35 (2012).
- [16] Mosley-Thompson, E., *et al.* Local to regional-scale variability of annual net accumulation on the Greenland ice sheet from PARCA cores. *J. Geophys. Res.* **106**, 33839-33851 (2001).
- [17] Tedesco, M., *et al.* Evidence and analysis of 2012 Greenland records from spaceborne observations, a regional climate model and reanalysis data. *Cryosphere* **7**, 615-630 (2013).
- [18] Koenig, L.S., Miège, C., Forster, R.R. and Brucker, L. Initial in situ measurements of perennial meltwater storage in the Greenland firn aquifer. *Geophys. Res. Lett.* **41**, 81-85 (2014).
- [19] Bezeau, P., Sharp, M., Burgess D. and Gascon, G. Firn profile changes in response to extreme 21st-century melting at Devon Ice Cap, Nunavut, Canada. *J. Glaciol.* **59**, 981-991 (2013).
- [20] Zdanowicz, C. et al. Summer melt rates on Penny Ice Cap, Baffin Island: Past and recent trends and implications for regional climate. *J. Geophys. Res.* **117**, F02006 (2012).
- [21] Gascon, G., Sharp, M. J., Burgess, D. O., Bezeau, P. and Bush, A. Changes in accumulation area firn stratigraphy and meltwater flow during a period of climate warming, Devon Ice Cap, Nunavut, Canada. *J. Geophys. Res.* **118**, 2380-2391 (2013).

- [22] de la Peña, S., *et al.* Changes in the firm structure of the western Greenland Ice Sheet caused by recent warming. *Cryosphere* **9**, 1203-1211 (2015).
- [23] IPCC, Climate Change 2013: *The Physical Science Basis. Contribution of Working Group I to the Fifth Assessment Report of the Intergovernmental Panel on Climate Change*. T. Stocker, et al. Eds., Cambridge, United Kingdom and New York, NY, USA: Cambridge University Press (2013).
- [24] McGrath, D., Colgan, W., Bayou, N., Muto, A. and Steffen, K. Recent warming at Summit, Greenland: Global context and implications. *Geophys. Res. Lett.* **40**, 2091-2096 (2013).
- [25] Liang, Y., *et al.* A decadal investigation of supraglacial lakes in West Greenland using a fully automatic detection and tracking algorithm. *Remote Sens. Environ.* **123**, 127-138 (2012)
- [26] Howat, I.M., Negrete, A. and Smith, B.E. The Greenland Ice Mapping Project (GIMP) land classification and surface elevation data sets. *Cryosphere* **8**, 1509-1518 (2014).

## Acknowledgments

This work is supported by the US National Aeronautics and Space Administration (NASA) Grant #NNX10AR76G, "Comprehensive Assessment of Ice Sheet Contributions to Sea Level Based on Integrated Remote Sensing Observations", by the Greenland Analogue Project (GAP), funded by Svensk Kärnbränslehantering AB, Sweden, Posiva Oy, Finland, and NWMO, Canada, the Refreeze Project funded by GEUS, the RETAIN project, funded by the Danish Council for Independent research (Grant #4002-00234) and the Programme for Monitoring of the Greenland Ice Sheet (PROMICE), funded by The Danish Energy Agency DANCEA programme. Collection and analyses of the legacy cores was supported by NASA's PARCA Program. The K-transect program has been funded by Utrecht University, the Netherlands Polar Program of NWO/ALW and a Spinoza grant. This publication is contribution number 62 of the Nordic Centre of Excellence SVALI, "Stability and Variations of Arctic Land Ice", funded by the Nordic Top-level Research Initiative (TRI). The authors acknowledge field assistance by K. Alley, A. Crawford, S. Doyle, M. Eijkelboom, S. Grigsby, D. Hill, A. Heilig, A. Hubbard, K. Lindbäck, R. Petterson and M. Stevens as well as logistical contributions from W. Abdalati, R. Bauer, A. Hubbard and T. Scambos. Satellite imagery in Supplementary Figure 1 is subject to copyright by European Space Imaging / DigitalGlobe.

### **Author Contributions**

H.M. conceived the study; M.M., D. vA. and H.M. collaboratively designed and planned the field campaigns in which M.M., H.M., D. vA., C.C. and W.C. participated; H.M., M.M., D. vA., J.B. C.C., W.C., R.S.F and E.M-T. performed the data analysis, E.M-T., R.S.W.vW. and Ha.M. prepared and provided additional data. H.M. and M.M. wrote the manuscript; all authors continuously discussed the results and developed the analysis further.

### **Author information**

The authors declare no competing financial interests. Correspondence and requests for materials should be addressed to H.M. (horst.machguth@geo.uzh.ch). The utilized legacy core data are available at <http://research.bpcrc.osu.edu/Icecore/data/>.

## Methods

### Field investigations

April 2009, two 3.5 m depth cores were obtained at 1840 m a.s.l. (Fig. 1 and Supplementary Fig. 1). At this site in early May 2012, three 10.5 m cores were obtained, firn temperature strings were installed (three to 10 m and one to 15 m depth) and a 1x1 km firn radar grid was recorded. Between 22 April and 22 May 2013, cores were extracted in 100 m elevation intervals between 1840 and 2360 m a.s.l. Nine of the fifteen cores were drilled to depths between 16 to 19 m. For all cores, stratigraphy and density was sampled at 1 and 10 cm resolution, respectively. A 110 km radar profile connects all cores of the transect and extends down to 1660 m a.s.l. One core at 1840 m a.s.l., one at 1927 m a.s.l. and two cores at 2466 m a.s.l., all drilled in May 2015, are also used here.

### Relating core stratigraphy to GPR data

A Malå 800 MHz shielded GPR Rx/Tx antenna was towed behind a snowmobile, recording traces every 0.5 seconds at a mean speed of 2.84 m s<sup>-1</sup>. 2024 samples were recorded at 0.10 ns intervals within each trace, for a total approximate depth of 20.5 meters. Latitude, longitude and elevation were recorded with a Trimble 5700 differential GPS at 1Hz. After preprocessing, GPR traces were resampled to 1.5 meter spacing and merged into a single transect. Ice lenses were identified using a local moving window to identify thick regions of refrozen ice with low signal variances. Additional processing details are provided in the supplementary information.

Comparison between radar and core stratigraphy confirms that the near-surface ice layer is continuous from ~1680 m a.s.l. to ~1870 m a.s.l. (Supplementary Fig. 3). We define the lower limit as the first appearance of underlying firn; and use an approximate definition for the upper limit where the near-surface layer separates into an upper and a lower ice horizon. The firn cores (Fig. 2) also confirm the separation into a sequence of thinner lenses.

### Statistically distinguishing firn regimes

We quantify the two firn regimes by investigating the change in available pore space  $p_t$  with depth  $h$ . We apply the Null hypothesis (Student's t-test), that the calculated slopes using the least square method of  $p_t(h)$  vs. depth for all nine 2013 cores are similar. The calculated slopes between the cores in the firn runoff regime are significantly ( $p < 1\%$ ) different from all the other cores but not

from each other ( $p = 28\%$ ). Cores in the percolation regime are not significantly different from each other ( $8\% < p < 92\%$ ).

### **Summer 2012 mass balance and retention at 1840 m a.s.l.**

At 1840 m a.s.l. (Supplementary Fig. 1) cores were obtained at Sites A and B (~250 m separation). At Site A *core\_1\_2012*, *core\_2\_2012* and *core\_1\_2013* were drilled within a ~50 m radius; *core\_3\_2012* and *core\_2\_2013* were drilled at a ~50 m horizontal displacement at Site B, compensating for the ice movement (~50 m year<sup>-1</sup>).

Cores from Sites A and B are grouped in three pairs of repeat-cores (Supplementary Fig. 4); for Site A the pairs are *core\_1\_2012/core\_1\_2013*, and *core\_2\_2012/core\_1\_2013*, and for Site B *core\_3\_2012/core\_2\_2013*. A visual comparison of the 2012 cores reveals distinct stratigraphic similarities. Evaluating changes from 2012 to 2013 indicates that firn density shallower than ~5.2 m increased substantially while below, the characteristic sequence of ice lenses and the density profile remained essentially constant. Depth values hereafter refer to the spring 2013 vertical coordinate system (Supplementary Fig. 4). Changes shallower than 5.2 m are attributed to the in-filling of firn pore space by infiltration and refreezing of meltwater. A pronounced refreezing event is documented by the firn temperature string data (Supplementary Fig. 5 and Discussion).

The unchanged lower sections of the density profiles below 5.2 m depth are used to align the pairs of cores using linear regression between the 2012 and 2013 profiles. The two density profiles in each pair of cores are displaced in 1 cm intervals and for each step the regression coefficient of the two profiles is calculated. The displacement for which correlation is at maximum is applied to align the pairs of cores (Supplementary Fig. 4). The aligned profiles are used to calculate the change in density  $\Delta\rho$  over the depth range where the 2012 and 2013 profiles overlap. The onset of the ice layer (marked with *EOMS*<sub>2012</sub> in Supplementary Fig. 4) is defined as the 2012 end of melt season (EOMS) surface.

Ablation is assumed equal to melt water production calculated from surface height lowering between spring 2012 and *EOMS*<sub>2012</sub>. Meltwater retention in 2012 is derived from integrating  $\Delta\rho$  below *EOMS*<sub>2012</sub>. Annual ablation (-0.99, -0.93 and -0.83 m w.e.) and retention (0.27, 0.29 and 0.14 m w.e.) values agree within 0.13 m w.e. among the three pairs. Ablation values are in good

agreement to two independent measurements of ablation (-1.00 and -0.91 m w.e., see Supplementary Discussion).

### **Changes in firn stratigraphy from spring 2013 to spring 2015 at 1840 m a.s.l.**

Using the same approach as described above, *core\_1\_2015*, drilled in May 2015 at the 1840 m site, is aligned to *core\_1\_2013* and *core\_2\_2013* (Supplementary Fig. 4). Both pairs of cores indicate accretion of ice on top of the thick ice lenses. With respect to the  $EOMS_{2012}$  reference horizon, accretion amounts to 0.49 m (*core\_1\_2013/core\_1\_2015*) or 0.63 m of ice (*core\_2\_2013/core\_1\_2015*). Integrating  $\Delta\rho$  over the depth ranges of accreted ice yields 0.20 and 0.31 m w.e. Integrating  $\Delta\rho$  below  $EOMS_{2012}$  yields also positive values (0.19 m w.e. and 0.1 m w.e.). To isolate the effect of melt water percolation and refreezing from the influence of natural firn compaction, the above values need to be reduced by roughly 0.01 m w.e. (for the depth range of accreted ice) and 0.06 m.w.e. (entire depth range below  $EOMS_{2012}$ ). Percolation and refreezing thus appear more active on top of the thick ice layers, as opposed to below. All calculated numbers, however, are subject to considerable uncertainty as the core comparison is hampered by 2015 sample consisting of only one core.

### **Maximum elevation extent of supraglacial rivers, 1985 to 2014**

We consider supraglacial rivers to be unambiguous expressions of surface runoff. Melt river maximum elevation ( $E_{max}$ ) extent for the time period 1985 to present is mapped in all 78 available Landsat images between 15 July and 31 August that cover the area between the 1840 m site and the ice sheet margin.  $E_{max}$  is defined as the average elevation of the five highest river heads (see Supplementary Discussion) in a 25 km wide interval north and south of the radar transect (cf. Fig. 1). The transect is linearly projected to the ice margin from its lower (1670 m a.s.l.) limit. Where more than one image per year exists, the one showing the highest melt river extent was considered (Supplementary Fig. 2). As outlined in Supplementary Discussion, we consider the Landsat analysis to reliably indicate that the melt river extent of the 2012 melt season stands out compared to all other years (cf. also [5,17]).

### **Contribution of 2012 firn-area runoff to total meltwater discharge**

The contribution of the firn area to total runoff in summer 2012 is calculated along the K-Transect, spanning an elevation range from the ice margin at 300 m a.s.l. to 2200 m a.s.l. The approach,

outlined in the following, avoids ambiguous delineations of ice sheet meltwater catchments<sup>27</sup> and provides a regional scale estimate. The computation requires knowledge of the elevation profiles of surface melt and hypsometry as well as the fractions of retained meltwater at the different elevations. The calculation incorporates a Monte Carlo (MC) framework to assess uncertainty.

- (i) The hypsometry along the K-Transect is calculated over a 10 km width, perpendicular to the K-Transect, in 100 m elevation bins over the 300 – 2200 m a.s.l. range using the 90 m horizontal resolution GIMP DEM<sup>26</sup>. The transect-length per elevation interval is then derived from area per elevation interval and width and expressed as a fraction of mean transect length. The derivative of the hypsometry is finally approximated using a linear regression ( $r^2 = 0.884$ ). See Supplementary Fig. 6.
- (ii) The elevation profile of ablation in the 2012 melt season is calculated based on in-situ measurements of annual surface mass balance along the K-transect<sup>6,15</sup>, and by means of firn core analysis (1840 m site, as outlined above). The latter allows retrieval of ablation from spring to autumn 2012. To isolate summer ablation from measured annual surface mass balance, the water equivalent of the snow cover that built up over the time period August 2011 to the onset of melt in spring 2012 is subtracted. Direct measurements of snow water equivalent at 1840 m a.s.l. indicated a 2012 pre-melt (early May) snow cover of 0.26 m w.e. Snow thickness measured at 1010 m a.s.l. (site-6 site, Fig. 1) is generally low (0.18 m on average from 2003 to 2015), at site-5 (490 m a.s.l.) snow is rarely present, corroborating limited accumulation at low elevations<sup>6,15</sup>. Hence, all annual mass balance values from  $> 800$  m a.s.l. were adjusted by  $c = -0.25$  m w.e. so the values reflect 2012 melt season ablation (Supplementary Fig. 6). As shown in Supplementary Fig. 6, melt is then approximated as a linear function of elevation ( $r^2 = 0.947$ ). Calculated melt is assumed the only source of water. Evaporation also modifies the surface water balance, however, the impact of rainfall and evaporation on water availability at the surface is small<sup>6</sup> and of opposite signs and thus the two processes are neglected.
- (iii) The firn meltwater retention is quantified by assigning fractions of retained meltwater ( $R_z$ ) for three characteristic elevation zones (Supplementary Fig. 6). Here a “zone” refers to elevation intervals and “area” refers to orographic units. For the elevation below the thick near-surface ice layers ( $< z_1 = 1680$  m a.s.l.) retention can be neglected<sup>7</sup>. For the ice



layer zone ( $z_l$  to  $z_t = 1870$  m a.s.l.)  $R_z$  is assumed to linearly increase from  $R_{z_l} = 0$  to  $R_{1840m} = 0.25$ , whereas the latter value refers to  $R_z$  measured at 1840 m in core data. No measurements of  $R_z$  are available for the area between  $z_t$  and an elevation  $z_m$  (2100 m a.s.l.) where all melt is assumed to be retained. A linear increase of  $R_z$  from  $R_{1840m} = 0.25$  to  $R_{z_m} = 1$  is assumed. The assumption of a linear increase of retention is based on the continuous decrease of ice layer thickness with elevation (Supplementary Fig. 3).

The linear regressions of hypsometry and melt are multiplied to weigh melt with normalized transect length at any given elevation. Integration over the three elevation intervals of characteristic meltwater retention (300 to 1680 m a.s.l., 1680 to 1870 m a.s.l. and 1870 m a.s.l. to 2100 m a.s.l.), and multiplication with the respective  $1 - R_z$  yields runoff from the three elevation zones.

Overall uncertainty in runoff contributions is computed by embedding the calculation in a MC framework according to<sup>28</sup>, repeated 5000 times while the parameters  $c$ ,  $z_l$ ,  $z_t$ ,  $z_m$ ,  $R_{1840m}$  are simultaneously varied according to their expected uncertainties (Supplementary Table 1) to account for interaction of individual parameter uncertainties. Uncertainty in the two linear regressions is quantified as the standard error of the regression slopes. Prior to each run the parameters are modified according to  $k_m = k + \xi\sigma_k$ , where  $\xi$  is a normally distributed random number whose values are centred at 0 with a standard deviation of 1,  $k$  stands for any of the parameters listed above and  $k_m$  is the modified parameter value. For each parameter  $k$  a new value of  $\xi$  is generated, i.e., uncertainties  $\sigma_k$  are considered independent.

In each run the modified parameters  $c$ ,  $R_{1840m}$  are tested for validity. If  $c$  becomes negative its value is set to 0. Whenever the runoff limit  $z_m$  lies above the elevation of zero melt  $z_{no\_melt}$  then  $z_m$  is lowered to  $z_{no\_melt}$ . To account for the observation that melt was abundant in summer 2012 to high elevations, all runs where  $z_{no\_melt}$  falls below an arbitrarily chosen elevation of 2100 m a.s.l. are discarded. 69% of all runs pass this evaluation. Supplementary Table 1 lists the contribution to total runoff from each elevation interval as well as the calculated uncertainties (one standard deviation).

### **Fraction of relict pore space**

At the 1840 m site the fraction  $f_t$  of transient (relic) pore space  $p_t$  in the firn column is quantified by comparing the measured transient firn density profiles  $\rho_t(h)$  to a reference dry firn profile  $\rho_{HL}(h)$

(Supplementary Fig. 7). The latter is calculated according to [8], based on mean annual air temperature (corrected for recent warming) and precipitation, assuming no melt. The total pore space available for melt storage is derived to  $p_{HL} = \int_{h_s}^{h_{pc}} \rho_i - \rho_{HL} dh$  where  $h_{pc}$  and  $h_s$  are the pore-close-off depth and the bottom of the snow pack, respectively, and  $\rho_i$  is the mean density of all 0.1 m core fractions consisting only of ice ( $873 \pm 25 \text{ kg m}^{-3}$ ). Subsequently  $p_t$  is calculated as  $p_t = \int_{h_s}^{h_{pc}} \rho_i - \rho_t dh$  and  $f_r = p_t/p_{HL}$ . The above calculations require knowing  $\rho_t(h)$  below the bottom depth  $h_m$  of the firn core. Based on data from nearby Site-J<sup>29</sup>, we here assume that  $f_r$  in-between the bottom depth  $h_l$  of the thick ice layers and  $h_m$ , is representative for the unmeasured depth range  $h_m$  to  $h_{pc}$  ( $h_{pc} = 54 \text{ m}$  according to  $\rho_{HL}(z)$  for a pore close-off density of  $830 \text{ kg m}^{-3}$ ). The entire calculation is embedded in a Monte Carlo framework to assess overall uncertainty (cf. Supplementary Table 2). Full details on the calculation of relict pore space fraction are provided in the supplement.

#### **Additional References Methods**

- [27] Lindbäck, K., Pettersson, R., Hubbard, A. L., Doyle, S. H., van As, D., Mikkelsen, A. B. and Fitzpatrick, A. A. (2015): Subglacial water drainage, storage, and piracy beneath the Greenland ice sheet, *Geophys. Res. Lett.* **42**.
- [28] Machguth, H., Purves, R.S., Oerlemans, J., Hölzle, M. and Paul, F. Exploring uncertainty in glacier mass balance modelling with Monte Carlo simulation. *Cryosphere* **2**, 191-204 (2008).
- [29] Kameda, T., *et al.* Melt features in ice cores from Site J, southern Greenland: some implications for summer climate since AD 1550. *Ann. Glaciol.* **21**, 51-58 (1995).